

Tuning birefringence by using two-dimensional photonic band structure

Xiao Xiao, Bo Hou, Weijia Wen,^{a)} and Ping Sheng

Department of Physics, Hong Kong University of Science and Technology, Clear Water Bay, Kowloon, Hong Kong

(Received 1 June 2009; accepted 16 September 2009; published online 28 October 2009)

Birefringence is an optical characteristic intrinsic to anisotropic materials. In the paper, we show the microwave birefringence can be tuned as a function of frequency by utilizing the band structures of a two-dimensional photonic crystal consisting of metallic cylinders arranged in a two-dimensional square lattice. By measuring the transmission and mapping the field inside of the sample, the birefringence was directly determined. An agreement between band structure calculations and experiment measurements was achieved, with the frequency at the center of transmission band showing the least birefringence and the frequency at the band edge exhibiting the most.

© 2009 American Institute of Physics. [doi:10.1063/1.3247584]

In the present study, we show that in two-dimensional (2D) photonic crystals the periodic structure can be utilized to tune the birefringence as a function of frequency, in the regime where scattering is significant. Thus both the form factor and the structure factor can affect the birefringence and the interplay between the two (e.g., for systems consisting of 2D photonic crystals composed of anisotropic materials) is envisioned to exhibit rich possibilities.

Exactly analogous to electronic systems,¹ photonic crystals,² and metamaterials^{3,4} are artificial structures relying on periodicity and local resonances for their manifest characteristics. When a photonic crystal is constructed according to different periodic patterns, the effective dielectric constant of the structure, evaluated at the long wavelength limit, can exhibit anisotropy⁵ and hence birefringence.⁶ Birefringence of liquid crystals is basic to its display functionality, and the birefringence of nanowires and 2D photonic crystals have been subject to intensive investigations.⁷⁻⁹ In this work we study the birefringence of 2D photonic crystals in the microwave regime, with focus on the frequency range where the wavelength is comparable to the lattice constant.¹⁰ As the birefringence is usually manifest as the existence of two wave fronts in the sample—the *O* (ordinary) beam and the *E* (extraordinary) beam—we demonstrate the existence of birefringence by mapping the phase of the local fields inside the sample that directly indicate the divergence of the two beams.¹¹ The angle of divergence between the two beams provides us with a means to relate the PC band structure and the strength of the birefringence. It is also shown that the doubly degenerate states can give rise to a disordered phase pattern.¹²

The 2D photonic crystal examined in our experiment consists of 9×9 metallic cylinders each 8 mm in diameter arranged with a lattice constant of 30 mm. The structure is illustrated in Fig. 1. Two horn antennas were used as the microwave source and receiver. The sample was placed in the middle of the two horns. For mapping the local phase distribution, the horn receiver was replaced by a small dipole antenna (a dipolelike receiver), affixed so as to move along

the *x-y* plane, controlled by a computer. The local field's phase pattern inside the photonic crystal was scanned for the plane indicated in Fig. 1.

For a homogeneous sample with an anisotropic dielectric constant, the equation for the phase velocity may be expressed as⁶

$$\frac{s_1^2}{v_f^2 - v_1^2} + \frac{s_2^2}{v_f^2 - v_2^2} + \frac{s_3^2}{v_f^2 - v_3^2} = 0, \tag{1}$$

where $\vec{k} = k\vec{s}$, $|\vec{s}| = 1$, $v_i^2 = \omega^2/k^2$, $v_i^2 = 1/\mu_0\epsilon_i$, and s_i is the Cartesian component of the unit vector \vec{s} along the direction of the wave vector \vec{k} . From symmetry of our sample, we have $\epsilon_x = \epsilon_y = \epsilon_1 = \epsilon_\perp$ and $\epsilon_z = \epsilon_2 = \epsilon_\parallel$, where the subscripts \perp and \parallel means perpendicular and parallel to the cylindrical axis, respectively.

By solving Eq. (1), we obtain two solutions, denoted by superscripts (1) and (2)

$$v_f^{(1)2} = v^2 \quad \text{and} \quad v_f^{(2)2} = \sin^2\theta v'^2 + \cos^2\theta v^2, \tag{2}$$

where θ is the angle between the incident wave's propagating direction and the *z*-axis, $v^2 = v_x^2 = v_y^2 = 1/\epsilon_1\mu_0$ and $v'^2 = v_z^2 = 1/\mu_0\epsilon_2$. The optical axis is defined as the direction along which the phase velocities of both the ordinary beam (denoted as *O*, with velocity $v^{(1)}$) and the extraordinary beam (denoted as *E*, with velocity $v^{(2)}$) are the same. Accordingly, the *z*-axis is the optical axis of our sample.

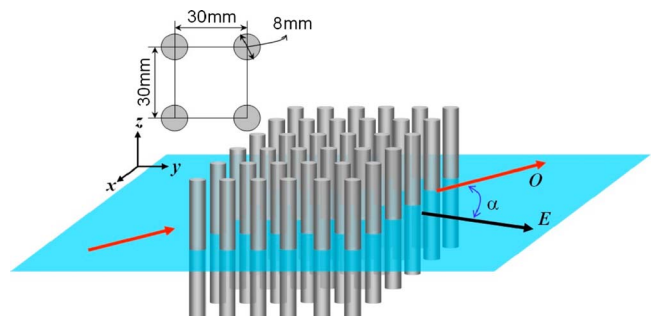


FIG. 1. (Color online) Schematic drawing showing the sample geometry with the measurement configuration.

^{a)}Author to whom correspondence should be addressed. Electronic mail: phwen@ust.hk.

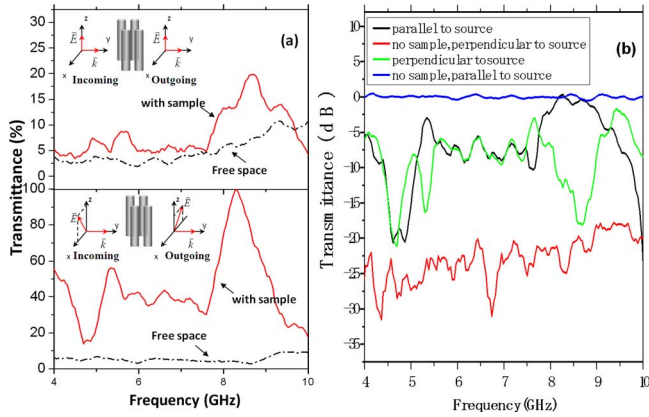


FIG. 2. (Color online) (a) Transmittance plotted as a function of frequency, measured with crossed polarizations for the source and the receiver. The geometry of the source and receiver polarizations is illustrated by the insets (where the red arrows indicate the polarization). For both the top and bottom panels, the red lines indicate the transmittance with the sample; the black dotted lines show the transmittance without the sample. For the top panel, the polarization of the source is parallel to z -axis, whereas for the bottom panel, it is at 45° with respect to the z -axis. (b) Transmittance in logarithmic scale plotted as a function of frequency for the different incident states. Here the blue and red lines are for transmittances without the sample, with the polarization of the receiver parallel (blue) and perpendicular (red) to that of the source. They serve as the reference. The black and green lines show measured transmittance with the sample, in which the polarization of the source makes an angle of 45° with the z -axis, and the polarization of the receiver is either parallel (black) or perpendicular (green) to the z -axis. The divergence of the black and green curves indicates birefringence. All the results were normalized to the case of free space with parallel polarizations of source and receiver.

We employ the Finite-Difference Time-Domain (FDTD) approach, which is particularly good at handling dispersive media such as metal.¹³

To obtain the band structure, we use random initial data at discrete nodal points in the unit cell, and propagate the fields forward in time by using the Maxwell equation with the perfect metallic boundary condition at the rod surfaces (which is an excellent approximation for waves in the microwave regime) and the Bloch boundary condition at the cell boundaries

$$\vec{E}(\vec{r} + \vec{R}_n) = e^{ik \cdot \vec{R}_n} \vec{E}(\vec{r}), \quad (3)$$

where \vec{E} denotes the electric field, \vec{k} is the Bloch wave vector in the first Brillouin zone, and \vec{R}_n is the lattice vector of the unit cell. After running the FDTD code for a sufficient long time, the time series $\vec{E}(t)$, summed over all the points in the unit cell, is Fourier-transformed into the frequency domain.¹⁴ The peaks in the frequency domain denote the frequency values corresponding to the particular chosen \vec{k} .¹⁵

In our experiment, the transmission spectra were first measured by setting the receiver's E -polarization perpendicular to that of the source [see the top illustration in Fig. 2(a)]. In this case, free space gives very low signal as expected, shown by the black line. When the sample was placed between the two horns (red line), a weak transmission peak appeared at 8.3 GHz. By maintaining the orthogonality of the source and receiver polarizations but rotating the source horn's E -polarization to 45° from the optical axis (the z -axis) of the sample, the amplitude of transmittance increased rapidly to 100% at 8.25 GHz. We conclude that for

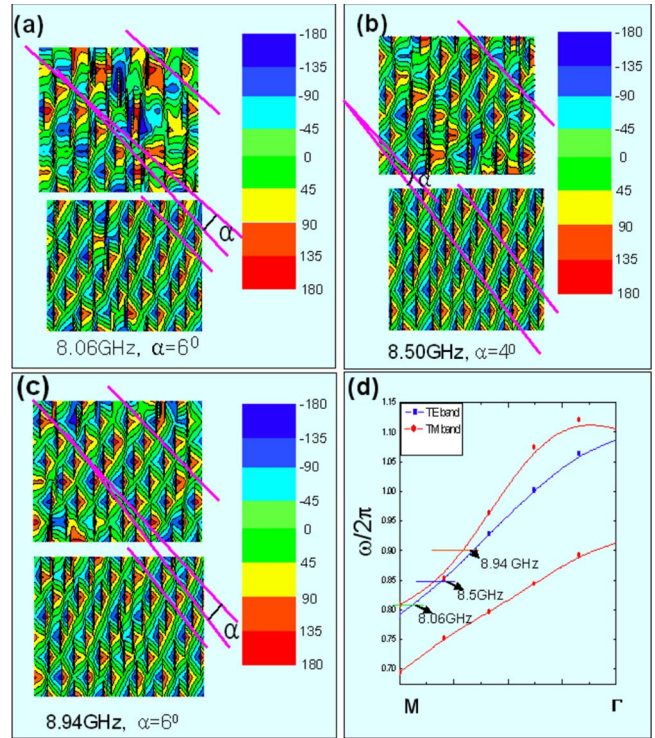


FIG. 3. (Color online) Local field mapping for the 2D photonic crystal with rod diameter 8 mm and lattice constant 30mm at three different frequencies: (a) 8.06, (b) 8.50, and (c) 8.94 GHz. The calculated band structure is shown in (d). Here the color scheme indicates the range of the measured phase, shown in the legend. The top panels in [(a)–(c)] are for the E -component (TM mode), and the bottom panels are for the O -component (TE mode). The straight magenta lines indicate the lines of constant phase. Their angular difference between the top and bottom panels gives a direction visualization of the birefringence.

the case illustrated at the top panel of Fig. 2(a), the birefringence is much weaker than it is in the case illustrated at the bottom of Fig. 2(a). In theory, for the top case, the birefringence should not occur. Hence the appearance of a peak is probably due to the misalignment of the cylinders in the crystal as well as sample's finite size. We also note from Fig. 2(a) that the optical axis of our sample is indeed parallel to the z -axis.

To observe the differences between the O -component and the E -component for polarized incident wave, we set the polarization of the source at 45° angle to the z -axis, whereas the polarization of the receiver was first set parallel (to detect the E -component) and then perpendicular to the z -axis (to detect the O -component). The measured transmission spectra are given by the four curves in Fig. 2(b). The birefringence phenomenon is indeed confirmed by the divergence of the green and black curves at a number of frequencies. Moreover, it is clear that the birefringence is highly frequency dependent.

We have calculated the band structure of our sample, shown in Fig. 3(d). It is seen that there is a stop band from 7 to 8 GHz for the TE mode.

In order to have a visible image of the birefringence, we designed and constructed a set of scanning devices for local field mapping inside of the sample. This could easily be realized by means of moving a dipole antenna throughout the plane indicated in Fig. 1. LABVIEW software was used to

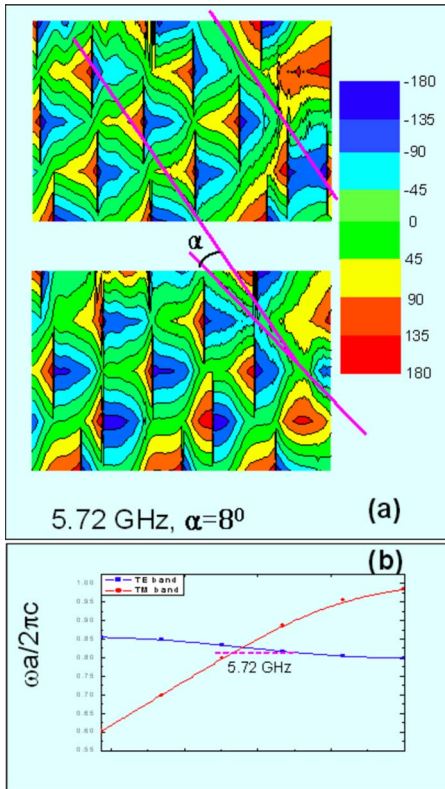


FIG. 4. (Color online) (a) Local field mapping for the 2D photonic crystal with rod diameter 25mm and lattice constant 43mm for incident wave at 5.72 GHz. The color scheme has the same meaning as that in Fig. 3. The top panel is for the *E*-component (TM mode) and the bottom panel is for the *O*-component. (b) Calculated band structure. The large separation between the dispersion relations of the TM (*E*) and TE (*O*) modes is seen to translate a large angular divergence of 8° seen in (a).

control the dipolelike receiver to detect the local field at 250 different points in intervals between the rows parallel to the *y*-axis of the sample. The incident wave was set at an angle, ranging from 35° to 45° relative to the *x*-*z* plane, as shown in Fig. 1. During the measurement, the polarization of the source was maintained at a 45° angle to the *z*-axis. The measurement was carried out as follows. First we set the dipolelike receiver, with its polarization parallel to the *z*-axis in order to detect the *E*-component. The phase patterns are plotted in the top panels of Figs. 3(a)–3(c) and 4(a). Next we changed the polarization of the dipolelike receiver to being perpendicular to the *z*-axis in order to detect the *O*-component. These phase patterns are plotted in the bottom panels of Figs. 3(a)–3(c) and 4(a) with the same color scheme as the top panels. Such field mappings were done for a number of frequencies ranging from 8 to 9 GHz, just above the stop band for the TE mode. Birefringence may be deduced by comparing the *O* and *E* patterns. In particular, an angle of separation for the two components can be explicitly measured, as shown in Figs. 3 and 4.

From the local phase mappings, we found the magnitude of the birefringence to be smallest in the middle of the transmission band. It is also found that the local field mapping for the TM mode (the *E*-component) [see top illustrations in Figs. 3(a)–3(c)] displays more disorder in the field pattern at the lower end of the frequency range. We elaborate on these two points below.

From our calculated band structure it is found that the magnitude of the birefringence is directly related to the separation between the TE mode (the *O*-component) and the TM mode (the *E*-component) at the same frequency—larger the separation, larger the magnitude of the birefringence. Thus in Figs. 3(a)–3(c) we see that as the frequency increases from 8.06 to 8.50 to 8.94 GHz, the angle of deviation between the two modes varies from 6° to 4° and then back to 6° . This variation is noted to correspond very accurately with the band structure predictions, based on the separation between the TE and TM modes, as shown in Fig. 3(d).

The field mapping shown in Fig. 3(a) is also noted to display disorder. This is due to the fact that over a considerable range of frequencies there are two TM modes as shown in the band structure, Fig. 3(d). Because of this degeneracy, the two states inevitably interfere with each other, leading to the “disorder” seen in the field pattern. However, as one of the TM mode’s dispersion curves displays a (upper) band edge at the Γ point, its wavelength is inevitably larger, implying a much less disordered field pattern at the higher (8.94 GHz) frequency range.

We have also studied another sample comprising a 6×6 simple square lattice composed of metallic cylinders with diameters of 25 mm and lattice constant of 43 mm. The local field distribution, mapped using the same approach as before, is shown in Fig. 4(a). The pertinent band structure is shown in Fig. 4(b). From the separation between the TM and TE modes at the same frequency, we find that at 5.72 GHz there can be a fairly large birefringence. Indeed, from the field pattern shown in Fig. 4(a) the birefringence in this case is larger than those found in the previous sample comprising smaller-diameter cylinders.

Financial support from Hong Kong RGC Grant Nos. 603207 and HKUST3/06C is hereby gratefully acknowledged.

- ¹J. D. Jackson, *Classical Electrodynamics*, 3rd ed. (Wiley, New York, 1999).
- ²J. D. Joannopoulos, P. R. Villeneuve, and S. Fan, *Nature (London)* **386**, 143 (1997).
- ³D. R. Smith, J. B. Pendry, and M. C. K. Wiltshire, *Science* **305**, 788 (2004).
- ⁴P. Sheng, *Science* **313**, 1399 (2006); J. Pendry, *Nature Mater.* **5**, 599 (2006).
- ⁵B. Hou, H. Xie, W. Wen, and P. Sheng, *Phys. Rev. B* **77**, 125113 (2008).
- ⁶M. Born and E. Wolf, *Principles of Optics*, 7th ed. (Cambridge University Press, Cambridge, England, 1999).
- ⁷O. L. Muskens, M. T. Borgstrom, E. P. A. Bakkers, and J. Gomez Rivas, *Appl. Phys. Lett.* **89**, 233117 (2006).
- ⁸F. Rutz, T. Hasek, M. Koch, H. Richter, and U. Ewert, *Appl. Phys. Lett.* **89**, 221911 (2006).
- ⁹F. Genereux, S. W. Leonard, H. M. Van Driel, A. Birner, and U. Gosele, *Phys. Rev. B* **63**, 161101(R) (2001).
- ¹⁰J. B. Pendry, A. J. Holden, W. J. Stewart, and I. Youngs, *Phys. Rev. Lett.* **76**, 4773 (1996).
- ¹¹A. L. Pokrovsky and A. L. Efros, *Phys. Rev. B* **65**, 045110 (2002).
- ¹²A. A. Krokhin, E. Reyes, and L. Gumen, *Phys. Rev. B* **75**, 045131 (2007).
- ¹³J. H. Choe, Q. H. Park, and H. Jeon, *Curr. Appl. Phys.* **9**, 18 (2009).
- ¹⁴K. Sakoda, N. Kawai, T. Ito, A. Chutinan, S. Noda, T. Mitsuyu, and K. Hirao, *Phys. Rev. B* **64**, 045116 (2001).
- ¹⁵A. Taflov and S. C. Hagness, *Computational Electrodynamics—The Finite-Difference Time-Domain Method*, 3rd ed. (Artech House, Boston, 2005).